Thermal degradation analyses of carbonate solvents used in Li-ion batteries

Y. Fernandes, A. Bry, S. de Persis

Thermal degradation analyses of carbonate solvents used in Li-ion batteries

Y. Fernandes[1,2], A. Bry[1] and S. de Persis*[2]
[1]CEA Le Ripault, BP 16, 37260 Monts, France
[2]ICARE, CNRS, University of Orléans, 1C, avenue de la recherche scientifique, 45071 Orléans Cedex 2

*corresponding author

Yann Fernandes

CEA Le Ripault BP 16, 37260 Monts, France

02 47 34 58 48

yann.fernandes@cea.fr

Alain Bry

CEA Le Ripault BP 16, 37260 Monts, France

02 47 34 40 04

alain.bry@cea.fr

Stéphanie de Persis*

ICARE – Institut de Combustion Aérothermique Réactivité Environnement

UPR3021 CNRS-INSIS

Université d'Orléans – Collegium Sciences et Techniques

1C, avenue de la Recherche Scientifique

CS 50060

45071 Orleans Cedex 2

Phone : +33.2.38.25.54.88 Fax : +33.2.38.69.60.04

Email : stephanie.de_persis@cnrs-orleans.fr

1. Introduction

The development of lithium-ion batteries is the result of a compromise between many parameters, such as electrical performance, longevity, weight/power ratio, industriability, manufacturing cost, or even user safety and environment safety. This last point is currently being studied post-development, during tests known as abusive tests, in which the limits of use of the object are sought. Ensuring the safety of lithium-ion batteries in use, especially in accident situations, is a key issue for their deployment in embedded systems (automotive, aviation, ships, etc.). Many abusive tests (mechanical, thermal, or electrical) lead to the emission of gases whose quantity and nature depend on the design of the electrochemical storage system: the nature of the substances used (electrolytes, in particular) and the architecture chosen (security devices, in particular). The precise identification and dosage of the gas emission composition are hurdles that currently still need to be overcome for Li-ion batteries. Artificial aggressions, such as an electric overcharge, are of particular interest since this test leads to one of the strongest reactions of the cell [*1*]: a steep increase in temperature, quasi-systematic opening of the cell envelope, and fume emissions in large quantities or even ignition of the envelope. Currently, there is a strong demand for this type of aggression from designers of energy storage devices in the form of Li-ion batteries and from users, in order to characterize the nature and origin of the gases thus formed. Despite the extensive literature on abusive tests, few studies relate to tests coupled to a gas analysis [2-22] and even fewer studies present quantitative results following an overcharge test [2,5,17,22]. However, it is of fundamental interest to study the link between the aggression and the gas emissions, in order to understand the reaction mechanisms involved. Better knowledge of the gases emitted would make it possible to guide the battery design substance choices upstream, and to improve the flammability aspect after deconfinement downstream. In our previous study [22], overcharge tests coupled with the identification and quantification of the gases emitted following the deconfinement of a commercial Li-ion cell were made, using two assemblies allowing the analysis of the gases emitted at the end of the test, and continuously during the test. The degassing analysis highlighted the important role of temperature in the volume of the gases created.

The aim of the present study was to assess the contribution of the thermal effect. To this end, the cell was decomposed into its constituents in order to decouple the phenomena responsible for the creation of gases. In particular, we have chosen to target the thermal degradation of the electrolyte solvents in an inert atmosphere since a review of the literature showed that both the graphite anode and the LFP cathode are thermally stable at the temperatures assumed to be reached in the overcharge tests [23,24] and are not directly the source of gaseous emissions. In addition, there are few studies including gas analyses that relate to the thermal degradation of carbonate solvents, which are typically encountered in commercial Li-ion batteries, either with or without a lithium salt, in an inert atmosphere. While similar thermal experiments have been carried out, their results are divergent and the conclusions reached sometimes inconsistent. Some experiments encountered difficulties due to thermal non-uniformity with cold points or non-isothermal kinetics, water effects, and HF loss for example. There is a general consensus, however, on the probable catalytic effect of $LiPF_6$ on the thermal degradation of solvents.

In this study, we focused on the development of an experimental setup to study the thermal degradation of electrolyte solvents without salt. We propose a device design to overcome the drawbacks listed by previous studies. This device was coupled with an analytical device allowing the identification and quantification of gases by gas micro-chromatography. These are presented in Section 3. The thermal degradation results are described and discussed in Section 4. Finally, the results were compared with those obtained in our previous study [22] on the analysis of gases emitted by a commercial cell during abusive overcharge tests.

2. Literature review

The first studies date back to the 1960s. In 1961, Wijnen [25] studied DMC pyrolysis in a quartz cylinder with a volume of 217mL, between 147 and 257°C, for an initial pressure ranging from 8.5 to 28mbar and for durations ranging from 300 to 3600s. The means of analysis was not described in the study. In all the experiments, CO_2 and CH_3OCH_3 were identified. In some experiments, those in which residual air was present despite evacuation, the presence of CH_3OH accompanied by an increase in the production of CO_2 was observed. To explain this, the author hypothesized that CH_3OH and CO_2 were formed by the hydrolysis (from traces of residual water) of the DMC. In 1962, Thynne and Gray [26] studied DMC pyrolysis in a 140-mL quartz cylinder heated in an oven. The operating conditions were the following: temperature range between 147 and 244°C, and initial pressure of 15.9 to 38.1mbar for durations between 1800 and 5520s. The analyses were carried out by gas chromatography (GC), coupled with a thermal conductivity detector (TCD). During their DMC pyrolysis experiments, Thynne and Gray identified and quantified the following products: CO_2 and CH_3OCH_3 in equivalent amounts. Their results confirmed those of Wijnen [25], namely that DMC pyrolysis over the temperature range of 147-257°C seems to preferentially form CO_2 and CH_3OCH_3. In 1965, Gordon and Norrish [27] studied DMC, DEC and EMC pyrolysis using a 45mL quartz tank as a degradation device and GC coupled with a GC/MS mass spectrometer for the analysis of the gaseous products. The DMC was pyrolysed in an oven at 350°C for 1200 seconds (20min) and photolysed at various temperatures up to 350°C, at an initial total low pressure in the tank (13.3mbar). The DMC did not decompose in either of the experiments (pyrolysis and photolysis). The presence of traces of CO, CH_4 and CO_2 was observed in the case of photolysis. Gordon and Norrish also studied the pyrolysis of DEC and EMC over the temperature range of 300-375°C for 600s (10min). The products identified were C_2H_4 and CO_2 in equimolar proportion in both cases. These products were accompanied by the formation of C_2H_5OH in the case of DEC and CH_3OH in the case of EMC.
Much later, in 2003, Botte et al. [28] analysed, in a calorimeter, the thermal degradation of an EMC/EC (ethylene carbonate) mixture, under an inert atmosphere, from 20 to 320°C, at a rate of 10°C·min^{-1}. They observed that EC becomes degraded at 263°C and that the EMC is stable up to 320°C. The non-condensable gases resulting from the degradation of the EC were analysed by GC and dosed by titration: CO_2 was the main gas quantified (15%) followed by traces of O_2 and H_2 (422ppm and 33ppm, respectively). The remaining 85% of the gaseous species could not be analysed, because they condensed in the calorimeter during the cooling stage prior to the analyses. They also studied the impact of adding dioxygen at different pressures (340mbar/690mbar/1030mbar/1380mbar) on the thermal stability of

EMC and found that it decomposed at between 220 and 235°C with this oxygen addition. The greater the O_2 concentration in the atmosphere, the higher the decomposition temperature, indicating that the EMC must reach a certain concentration in the gas phase before reacting with the oxygen. The authors also observed that the decomposition of EMC is accompanied by the production of carbon dioxide, but did not quantify it.

Ravdel et al. (2003) [29] studied the thermal decomposition of electrolytes composed of $LiPF_6$+DMC, $LiPF_6$+DEC and $LiPF_6$+EMC, sealed in glass ampoules in an oven at 85°C for 500 hours under an inert atmosphere. The glass ampoules were filled inside a glove box, in which the water content was less than 1 ppmv. The identification of the species resulting from this degradation was done by GC/MS. The products observed during the gentle pyrolysis of electrolytes were the following: i) $LiPF_6$+DMC: CO_2, POF_3, CH_3OCH_3, PF_5, $OPF_2(OCH_3)$; ii) $LiPF_6$+DEC: CO_2, POF_3, PF_5, CH_3OCH_3, $C_2H_5OC_2H_5$, $CH_3OC_2H_5$, $OP(OC_2H_5)F_2$, C_2H_5F, DMC, DEC; iii) $LiPF_6$+EMC: CO_2, POF_3, C_2H_5F, $C_2H_5OC_2H_5$, PF_5, $OP(OC_2H_5)F_2$, $OP(OC_2H_5)_2F$. Note that CH_3OCH_3 was only identified when the electrolyte contained DMC and EMC, $C_2H_5OC_2H_5$, C_2H_5F and $OP(OC_2H_5)F_2$ were identified in the case of the degradation of EMC and DEC.

In the 2003 study by Guanaraj [30], the thermal degradation under an inert atmosphere of a mixture of EC, DEC, DMC and a lithium salt $LiPF_6$ was performed at 40 to 350°C by adiabatic reaction calorimetry (ARC) at a heating rate of $2°C \cdot min^{-1}$. The analysis of the gaseous phase was carried out in different stages, without quantification, by nuclear magnetic resonance spectroscopy (NMR), diluted in a solution of CD_3CN, and by Fourier Transform Infrared Spectroscopy (FTIR). At 220°C, the gaseous phase analysis carried out by NMR revealed the presence of CH_3F, C_2H_5F and $OHCH_2CH_2F$. FTIR spectroscopy, also carried out at this temperature, showed the presence of CO_2, EC, C_2H_4 and PF_5. Heating was continued up to 350°C after extraction of the entire gaseous phase created at 220°C. The NMR analysis of the gas phase at 350°C revealed the presence of CH_3F, C_2H_5F and $OHCH_2CH_2F$. The analysis of the gaseous phase of the mixture heated directly to 350°C, without sampling at 220°C, showed the presence of CH_3F, C_2H_5F and CO_2. $OHCH_2CH_2F$ is therefore absent from the gaseous phase during the direct heating of the mixture to 350°C.

In 2015, Lamb et al. [31] studied the thermal decomposition of DMC, EC, DEC and EMC solvents, with or without $LiPF_6$, and the decomposition of binary mixtures of these solvents with the lithium salt. For each manipulation, 500mg of sample was inserted into a 10mL steel calorimetric pump, which was transferred to an ARC under a nitrogen atmosphere. The electrolyte or solvent samples were heated from room temperature to 405°C. The gases produced over time were monitored. The gases resulting from this degradation were analysed for non-binary solvent samples (DEC, EC, EMC, and DMC) with 1.2M$LiPF_6$. The results of this study showed that the more volatile the solvent, the less gas it produces during thermal aggression. Indeed, the authors observed that EMC and DMC (without a lithium salt) are stable and produce very little gas up to about 130-140°C, and that no additional amount of gas is produced between 140 and 405°C. The initial decomposition of the DEC was observed at 305°C, and that of the EC at 190°C. The authors hypothesised that the DMC and EMC vaporised before any decomposition occurred, and that this vaporisation consumed the energy that allowed the non-volatile solvents to become degraded. The total gas production of each of the 4 solvents was also monitored with the addition of 1.2M of $LiPF_6$. It was also observed that $LiPF_6$ catalyses the decomposition reactions of the solvents, except in the case of the mixture (DMC+1.2M$LiPF_6$), where the addition of 1.2M$LiPF_6$ lowered the initial DEC decomposition

temperature from 305°C (DEC only) to 170°C (DEC+1.2M$LiPF_6$). This also allowed the decomposition of the EMC from 175°C and the acceleration of the decomposition rate of the EC at 190°C. The total decomposition of the EC+1.2M$LiPF_6$ mixture was in the 190-250°C range, while the total decomposition of the EC alone was in the 190 - 420°C range. The decomposition gases resulting from the heating at 405°C of the 4 solvents separated with 1.2M of $LiPF_6$ were analysed by gas chromatography (the C_2H_4 was not analysed). For the mixture of $LiPF_6$ with the EC, DMC and EMC solvents, the main gas formed was always CO_2. The decomposition of the DEC with the lithium salt produced mostly C_2H_6 and CO_2 in approximately the same proportions. The minority products were: H_2 for the EC, C_2H_6 for the EMC, H_2 and C_2H_6 for the DMC, and C_2H_6 and H_2 for the DEC. HF was not detected in the decompositions of the four solvents with $LiPF_6$. The authors pointed out that the HF may have reacted before the *ex-situ* gas analysis.

In the study by Sun et al. (2016) [32], a laminar flow reactor coupled with a GC system was used to study DMC pyrolysis in Ar at various pressures (40/200/1040mbar). The flow reactor consisted of a quartz tube heated by wires at different temperatures. The pyrolysis product samples were taken downstream from the reactor, identified by GC/MS, and quantified by GC/TCD and by flame ionization detectors GC/FID. The temperature along the flow tube was measured using a thermocouple. This temperature was not uniform along the entire length of the flow tube (bell shape). The various DMC pyrolysis manipulations performed in this study were carried out within the temperature range (Tmax) of 569-1217°C. The molar fractions of the gaseous species resulting from the pyrolysis, sampled at the sampling point, were given as a function of the maximum temperature Tmax. The residence time varied with the temperature and the study pressure; the values calculated at 40mbar, 200mbar and 1040mbar within the temperature range were, respectively, between 9.3×10^{-3} and 1.2×10^{-2} s, between 4.9×10^{-2} and 6.8×10^{-2}s, and between 2.5×10^{-1} and 3.1×10^{-1}s. The pyrolysis products observed at the three test pressures were, in decreasing order of molar fraction: CO, CO_2, CH_4, C_2H_4, CH_3OCH_3, C_2H_6 and C_2H_2. Decreasing the total pressure in the reactor increased the DMC decomposition temperature from around 675°C at 1040mbar, to 825°C at 200 mbar and 875°C at 40mbar.

In 2017, Sun et al. [33] carried out a DEC pyrolysis study of the same nature as the previous one: the reactor, the analysis device and the pressure conditions (40, 200 and 1040mbar) were identical. The various DEC pyrolysis manipulations performed in this study were carried out within the maximum temperature range of 427-927°C. The pyrolysis products observed at the three test pressures were: C_2H_5OH, CO_2 and C_2H_4 in equivalent molar proportions. Decreasing the total pressure from 1040mbar to 40 mbar increased the DEC decomposition temperature. At 1040mbar, this decomposition started from about 500°C and, at 40mbar, from about 580°C.

In 2017, Bertilsson [34] analysed (but did not quantify) the fluorinated emissions of an electrolyte, consisting of $LiPF_6$ and various solvents, by a TGA (thermogravimetric analysis)/FTIR coupling. In this study, an electrolyte, consisting of a mixture of $LiPF_6$ with DMC/EA solvents, was heated under an inert atmosphere at the rate of 10°C·min^{-1} up to 200°C. A second manipulation consisted in heating, under an inert atmosphere, an electrolyte consisting of $LiPF_6$ and EC/VC solvents, at a rate of 10°C·min^{-1} up to 650°C. Both samples were prepared in a glove box with a water content of less than 6ppmv. In both cases, between 100 and 170°C, POF_3 and HF were identified. The characteristic bands of these products were preceded by IR bands of water between 80 and 180°C. The authors therefore concluded that the formation

of POF_3 and HF was due to the $LiPF_6$ lithium salt reaction with the traces of water present in the device (from the mounting surfaces, the samples, or the flushing gas).

3. Experimental part

3.1. Experimental device

The experimental device is shown in Fig.1: it consists of a Swagelok assembly equipped with a 304L stainless steel cylinder, associated with two sealed SS-4H bellow valves, with a total volume of 50mL. According to the manufacturer's data, it can resist a maximum temperature of 315°C (588K) and a maximum pressure of 68.9bar ($6.89x10^6$Pa). The vacuum within the device was created and checked before each manipulation (validation when the pressure is lower than $2x10^{-2}$mbar). The leakage rate of the assembly was then checked (validation when it was lower than $3x10^{-3}$mbar·s^{-1}).

In order to prepare the injection of the solvent, the assembly is equipped with a septum at the inlet of one of the two valves. This assembly is then connected by the other valve to a pipe network comprising gas inlets, pressure sensors and a vacuum pump. A vacuum is then created within the device, to reach a pressure of less than $2x10^{-2}$mbar. When this condition is met, the vacuum pump is isolated from the assembly. The solvent is then rapidly injected with a syringe into the assembly through the septum, which maintains the vacuum for the duration of the injection of all of the solvent (approximately equal to 5s). The valve equipped with the septum through which the solvent was injected is closed, and the pressure of the injected solvent is measured using a pressure sensor (range 1-1100mbar). Finally, argon (at a pressure of about 2bar) is injected in stages into the assembly, until it reaches atmospheric pressure. The total injected pressure (solvent+Ar) is measured by another pressure sensor (range 0.01-2.5bar). The assembly is allowed to stand for 45min for the mixture to homogenize. The assembly is then inserted between four massive iron blocks, each weighing 2.5kg, placed in a Heratherm OMH60-S oven. Once it has been inserted and the oven has been closed again, the oven temperature is set to the experiment temperature.

3.2. Analysis device

In order to separate, identify and quantify the gaseous species created by the degradation of the solvents in the gas phase, analyses were carried out with the SRA Instruments gas micro-chromatograph coupled with the Agilent Technologies mass spectrometer used and described previously in the analysis of the gas static test assembly [22]. The analysis was performed at a controlled temperature in the laboratory (20±3°C). The chromatographic separation was carried out with two MS5A molecular sieve columns (one flushed with an argon carrier gas, and the other with a helium vector gas), with an OV1 column and with a

PLOTQ column (both flushed with a helium vector gas). The four columns, each equipped with a thermal conductivity detector (TCD), can be installed in series with the mass spectrometer.

3.3. Operating conditions

The results of the overcharge tests carried out in our previous study [22] showed that most of the gas emission (59%) is composed of solvent vapours from the electrolyte. As a first step, the four solvents of the study cell were analysed by differential scanning calorimetry (DSC) to obtain, as a first approximation, their degradation temperatures in an inert and confined atmosphere. The DSC device used for the study is the Q200 from TA INSTRUMENTS. The solvents used, purchased from Sigma Aldrich, have, according to the supplier's data, purities equal to or greater than 99% (DMC:≥ 99%; EMC:99%; EC:99%; PC:99.7%). The samples were introduced into sealed gold-plated crucibles with an internal volume of 40µL and able to withstand a maximum pressure of 300bar. The crucibles were sealed under argon in a glove box with water and oxygen contents of less than 1ppmv. The crucibles were weighed, on a precision scale, before and after the injection of the solvents, in order to know the exact mass of sealed solvent. This mass was between 3.80 and 3.85mg for liquid solvents (DMC, EMC and PC) and between 2.58 and 2.92mg for the solid solvent (EC). The crucibles were also weighed after passing into the DSC to check their tightness during handling. Fig.2 shows the thermograms of the study solvents, that is to say, the heat flux curves obtained by differential scanning calorimetry with a temperature ramp of 20°C·min^{-1}. This ramp was chosen because it was close to the maximum external temperature increase rate observed in the previous study (22.4°C·min^{-1}) [22].

The thermograms in Fig.2 all show peaks corresponding to an exothermic decomposition process. The initial decomposition temperatures of the DMC (247°C) and the EMC (264°C) were the lowest, while those of the PC (316°C) and the EC (335°C) were the highest. Two decomposition temperature ranges were thus observed between the linear solvents and the cyclic solvents: respectively, 247-264°C and 315-335°C. The linear solvents, DMC and EMC, have a lower degradation temperature than the cyclic solvents, EC and PC, and are therefore potentially the first to degrade during a thermal runaway event.

As a second step, in order to determine the composition of the initial gaseous phase in the cell, it was necessary to compare the volatility of the various solvents contained in the electrolyte. To do this, the evolution of the vapor pressures of the various solvents of the cell, as a function of temperature, must be known. We chose to use Antoine's equation for linear solvents (DMC, EMC) [35] and the equation of Kulikov et al. (2001) [36] for cyclic solvents (EC, PC). The results (not shown here) show, as expected, that the vapor pressure of the various solvents increases with temperature. In addition, it can be noted that the linear solvents (DMC and EMC) are much more volatile than the cyclic solvents, PC and EC, over the temperature range studied, which makes it possible to clearly distinguish two orders of magnitude of volatility. Assuming that the liquid mixture of solvents, without lithium salt, is an ideal solution, it is possible to calculate the saturating vapour pressures of each solvent as a function of the temperature, taking into account their proportions in the electrolyte (data in table A in the additional files) by applying Raoult's law. From these results, the vapour pressures of each solvent are then compared in Fig.A in the

additional files. The results of the calculations in Fig.A show that the cyclic solvents, EC and PC, are in the minority. They constitute 0.7% of the gaseous phase at 180°C, 1.3% at 240°C, and 2.0% at 300°C. The linear solvents, DMC and EMC, make up the majority of this gas phase, with a relative proportion of about 70% of DMC and 30% of EMC. The initial gaseous phase of the cell is thus assumed to consist solely of DMC and EMC. These are the two molecules that will be subjected to the highest temperatures and will potentially decompose. This observation, associated with the composition of the vapours above a heated electrolyte, reveals the possibility of a particular reactivity of the two linear solvents with respect to the cyclic solvents. The thermal degradation of the volatile solvents, DMC and EMC, was therefore studied. The operating conditions selected from the results of the global tests [22] and DSC analyses were the following: i) durations of 30min, 60min and 120min; ii) temperatures of 180°C, 240°C and 300°C. Each degradation test was duplicated, which represents a total of 18 manipulations per solvent. Each result presented in this study is based on the average of the two manipulations performed under the same time and temperature conditions. No significant difference in the nature and quantity of the products formed was observed between the two measurements. In order to verify that the assembly does not become thermally degraded and that no species creation takes place when it is heated in an oven, the device was filled with argon at atmospheric pressure and then insulated and heated in the oven for 4 hours at 300°C. The analysis resulting from this manipulation (not shown here) showed that no gaseous species were created. Therefore, it can be concluded that the degradation device does not produce gases and is thermally stable. The solvents used come from Sigma Aldrich. The DMC, which is anhydrous, has a purity greater than or equal to 99% and the EMC (non-anhydrous) has a purity of 99%. To dehydrate the EMC, dry molecular sieve beads were inserted into it. The absence of water in these two solutions was verified by injecting these solvents into the DRA gas micro-chromatography device.

In order to know the time necessary for the device atmosphere to reach the temperature of the experiment, calibrations were carried out. A thermocouple was introduced into the assembly, filled up to 1 bar with argon, via a septum, to monitor the internal temperature for each setpoint temperature. These results are shown in Fig.B in the additional files. The initial time (t_0) of the experiment was defined as the time when the temperature of the bottle atmosphere is 5 °C lower than that of the set point: it is t_0=800s for the three experiment temperatures (see Fig.B in the additional files). The device is thus maintained at the set temperature for the duration of the experiment. When the heating time for the experiment ends, the device is taken out of the oven and immediately cooled in a sand bath, in order to stop the reactions. The analysis of the gaseous species resulting from the degradation is done when the assembly atmosphere has returned to ambient temperature. Between each manipulation, the assembly is evacuated and then opened and dried in an oven to allow the desorption of any possible residual substances.

4. Results and discussion

4.1. Quantification protocol

The thermal degradation of solvents in the gas phase is likely to produce many molecules that must necessarily be separated chromatographically to be identified and then dosed. An analytical protocol was developed based on preliminary DMC and EMC degradation manipulations carried out for 2 hours at 300 °C. Upon each injection, the temperature and the pressure of the column were optimized in order to obtain an optimal separation of the peaks corresponding to the gaseous species created. This protocol resulted in the final method described in Table 1. Quantification was performed from experimentally obtained calibration curves (Fig.C in the additional files), on each of the columns, within the concentration range studied, with the analytical method outlined in Table 1 by a procedure similar to that detailed in [22]. The CH_4, N_2 and H_2 were calibrated from Alphagaz 2 Air Liquide gas cylinders. The CO_2 was calibrated from an Air Liquide gas cylinder with a volume concentration of 10.02±0.2% of CO_2 diluted in helium. CH_3OH was calibrated with a standard gas prepared from injections of different volumes of VWR methanol of purity greater than or equal to 99.9%. The DMC and EMC were calibrated in the same way as the methanol from the solutions used for thermal degradation. The concentrations of the other non-calibrated species were determined by adjusting their proportionality coefficient, when available, as a function of their thermal conductivity difference relative to the reference species calibrated at the analysis temperature. The identification of the unknown species was carried out by mass spectrometry using the same methodology as that used in our previous study [22]. The calculations for estimating the quantity of degraded solvent were done from the quantification of the species created by this degradation according to the methodology presented in the additional files with Fig.C. The pyrolysis kinetics may be influenced by the nature and surface area of the reactor walls [37, 38] (see Additionnal File).

4.2. Thermal degradation of DMC

A DMC volume of 5.5µL was injected into the 50mL assembly for each of the 18 DMC degradation manipulations. This volume makes it possible to remain below the saturation vapour pressure of the DMC at room temperature (80 mbar at 25°C [39]) and thus to ensure that all of the DMC is in a gaseous form in the assembly at the analysis temperature. In addition, this small injected volume makes it possible to limit the quantity of condensable gaseous species formed after thermal degradation, and therefore potentially difficult to quantify at 20°C. The average initial DMC pressure detected by the pressure sensor during the 18 was 33.3±1.4 mbar.

The manipulations were validated by performing a mass balance. The empirical formula of DMC is $C_3H_6O_3$, the sum of the products formed through its degradation must therefore be present in the following proportions: n(O*created*)/n(C*created*)=1 and n(H*created*)/n(C*created*)=2. Table 2 reports the values of these relations in the different manipulations.

It can be noted that, according to Table 2, there is a good match between the n(O)/n(C) and n(H)/n(C) theoretical and experimental ratios. However, there is a slight oxygen and hydrogen surplus that can be explained by a possible contamination of the device with H_2O and/or minority gases, such as CO. Indeed, residual species remain in the devices initially containing atmospheric air and then placed under vacuum (≈ 10^{-3}mbar), with about 75 to 85% of water vapour content in this residual atmosphere.

All the species observed in the chromatograms (presented in Fig.D of the additional files) were quantified by integrating their peaks. The quantification of CH_3OH and CH_3OCH_3 was carried out in column OV1 because these two species are not separated in column PLOTQ with the method used. The thermal degradation rates of the DMC were estimated for the various operating conditions, and are summarized in Table 3. As shown in Table 3, decomposition of the DMC in the gas phase was observed at the three study temperatures. This decomposition is slight when it is degraded at 180°C (from 1.12 to 3.12%), but becomes more significant at 300°C and when the degradation time is maximum (42.13%). It is about 3.5 times greater at 240°C than at 180°C, and 4 times higher at 300°C than 240°C.

Fig.3 shows the evolution of mole fractions of each species formed during the degradation of the DMC, based on the degradation time for the three study temperatures: 180°C, 240°C and 300°C. -Fig.3a) shows that irrespective of the duration, at the temperature of 180°C the DMC is mainly composed of CO_2 (≈ 47%), CH_3OCH_3 (≈ 32%), and CH_3OH (≈ 19%). H_2 and $CH_3OC(=O)H$ are formed in a small amount at this temperature. The variation in the duration of the degradation does not seem to affect the nature and proportion of the products. Figure3b) shows that at a temperature of 240°C, the DMC decomposes mainly into CO_2 (between 35 and 42%) and CH_3OCH_3 (between 24 and 33%). CO and H_2 are also produced in non-negligible quantities (between 10 and 14% for CO and between 5 and 11% for H_2). The proportion of CH_3OH decreases compared to the manipulations carried out at 180°C (approximately 14% at 240°C and 19% at 180°C). The CO and H_2 mole fractions increase compared to those at 180°C and represent about 20% of the total proportion of gaseous species created at this temperature. The duration of the degradation does not change the nature of the degradation products, but seems to change their proportions. This behaviour is particularly visible for CH_3OH and CH_3OCH_3, the production of which appears to be reversed. It can be due either to an artefact, in the case of the degradation manipulations carried out over the duration of 30 minutes, or possibly to pollution by wall water for these two manipulations compared to the other manipulations, resulting in the preferential formation of methanol. The proportions of CH_4, H_2 and CO increase with the duration of the degradation, while that of CO_2 decreases with the degradation time. As shown in Fig.3c, at the temperature of 300°C and whatever the duration, the four species mostly formed are CO_2 (≈ 28%), CH_3OCH_3 (between 20 and 24%), CO (≈ 21%) and H_2 (≈ 18%), and the three minority species are: CH_3OH (≈ 7%), CH_4 (≈ 4%), and $CH_3C(=O)H$ (≈ 0.5%). The proportion of CH_3OCH_3 formed appears to be influenced by the degradation time, with a maximum production observed for a duration of 60 minutes, just as in the manipulations carried out at 240°C. The proportions of H_2 and CO formed increase compared to those obtained at 240°C, while those of CO_2 and CH_3OCH_3 decrease in the total gas production.

4.3. Thermal degradation of EMC

The same thermal degradation and gaseous species analysis protocol was followed to carry out the EMC pyrolysis study. To ensure that the EMC is in gaseous form in the 50mL assembly, the injected volume was 3.2µL. The mass of EMC injected into the assembly is therefore approximately half that of the DMC. The average initial EMC pressure detected by the pressure sensor during the 18 manipulations was

16.9±0.7mbar. The formula for EMC is $C_4H_8O_3$, the sum of the products formed in its degradation must therefore include the following relations: n(O*created*)/n(C*created*)=0.75 and n(H*created*)/n(C*created*)=2. Table 4 gives the values of these relationships for various operations. It should be noted that there is a good agreement between the theoretical and experimental ratios. Nevertheless, there is a slight apparent surplus of hydrogen and oxygen, as in the case of the DMC thermal degradation manipulations.

The thermal degradation of EMC in gaseous form was observed at all three study temperatures. Table 5 shows the EMC mass loss values for the different experiments. EMC decomposition increases by about a factor of 6 between 180 and 240°C and by a factor of 2 between 240 and 300°C. This increase is greater than in the case of DMC (factor of 3.5) between 180°C and 240°C, and smaller between 240°C and 300°C (factor of 4).

The quantification was performed from the chromatograms obtained (an example of which is shown in Fig.E in the additionnal files). For methanol, quantification was carried out on the peak common to CH_3OH and CH_3OCH_3 of the PLOTQ column, by subtracting the CH_3OCH_3 contribution quantized in the OV1 column. Fig.4 shows the evolution of the mole fractions of each species formed during the degradation of EMC, as a function of the degradation time at all three temperatures studied. As shown in Fig.4a, at 180°C, and for a heating time of 30 minutes, CO_2 and C_2H_5OH are the main species formed; these species represent about 60% of all species created. The other species formed (in proportions greater than 5%) are: DEC, CH_3OH and DMC. The increase in the heating time causes the reduction of the molar fractions of CO_2 and C_2H_5OH, while those of DMC and DEC increase. This result is in good agreement with the study by Ravdel et al. (2003) [29] which showed that heating EMC with $LiPF_6$ at 85°C for 48 hours under an inert atmosphere leads to the production of DMC and DEC in concentrations higher than the other degradation products, due to the preponderance of the ester exchange reaction (2EMC→DMC+DEC) compared to decomposition reactions of EMC at this temperature.

Fig.4 shows that the CH_3OH formed appears to degrade over time because it represents 14% of all the products formed after 30 minutes of degradation, whereas it represents 6% after 2 hours. H_2, CH_3OCH_3, $CH_3C(=O)H$ and $CH_3OC_2H_5$ are produced in small amounts (less than 5%) in the EMC pyrolysis at 180°C. The proportions of all of these species increase with the duration of the degradation, except for $CH_3C(=O)H$. As shown in Fig.4b), at 240°C and for a heating time of 30 minutes, the majority species are CO_2, C_2H_5OH, DMC and DEC. These four species are present in the same proportions for all the manipulations as those carried out for 2 hours at 180°C. The minority species formed at 240°C are similar to those encountered at 180°C, with the addition of C_2H_4 and CO. The same trend is observed at 180°C: the molar fractions of C_2H_5OH, CO_2 and CH_3OH decrease when the heating time increases, while those of DMC and DEC solvents increase, respectively, from 19 to 29% and from 22 to 44%, between 30 and 120min. As shown in Fig.4c), at a temperature of 300°C, CO_2 (≈ 22%) is the main species formed, followed by DEC (≈ 17%) and DMC (≈ 15%). The proportions of DMC and DEC formed are fairly stable for the three heating times at 300°C, which was not observed in the case of handling at 180 and 240°C, where the proportions of these two species increase with the duration of the heating. The molar fractions of H_2 and C_2H_4 increase considerably at this temperature with respect to the temperature of 240°C going, respectively, from about 2 to 7% and 0.5 to 5% for 30min of degradation. Extending the heating time reduces the molar fraction of C_2H_5OH (from 14 to 9% from 30min to 2h). Many new minority species are produced at this temperature:

CH_4, C_2H_6, C_3H_6, $C_2H_5OC_2H_5$ and $CH_3C(=O)OCH_3$. Fig.4 shows that the mole fractions of CH_3OH and C_2H_5OH formed at all three study temperatures decrease with increasing duration. This could indicate that the EMC thermal degradation products in turn decompose to form new species. According to the ester exchange reaction (2EMC→DMC+DEC), the amount of DMC produced must be equal to that of DEC. However, in our study, whatever the temperature, the proportion of DEC quantified is always greater than that of DMC. This could indicate that DMC is highly reactive and likely to decompose thermally, forming new products.

4.4. Comparison with the literature

Table 6 summarizes the products obtained from the thermal decomposition of the DMC and EMC as a function of the decomposition temperature. Thermal decomposition of solvents was observed for all three heating temperatures: 180, 240 and 300°C and for 3 periods: 30, 60 and 120min. Different species were identified and quantified at the three study temperatures. The thermal degradation of DMC produced CO_2, CH_3OCH_3, H_2, CH_3OH and $CH_3OC(=O)H$ as from 180°C. CO and CH_4 were produced as from 240°C. The main thermal degradation products of DMC at 300°C were: CO_2, CH_3OCH_3, CO and H_2. CH_3OH, CH_4 and $CH_3OC(=O)H$ were produced to a lesser extent at this temperature. The thermal degradation of EMC produced many species at all three temperatures studied, as shown in Table 6. At 180°C, it produced CO_2, CH_3OCH_3, H_2, CH_3OH, C_2H_5OH, DMC, DEC, $CH_3C(=O)H$ and $CH_3OC_2H_5$. CO and C_2H_4 were produced as from 240°C. CH_4, C_2H_6, C_3H_6, $C_2H_5OC_2H_5$ and $CH_3C(=O)OCH_3$ were produced as from 300°C. At 300°C this thermal degradation was mainly the source of the CO_2, DMC, DEC, C_2H_5OH, H_2, CH_3OH and C_2H_4.

DMC and EMC thermal degradation reaction schemes, established from the global reactions (between stable species) referenced in the literature [25, 27, 29, 30, 40-49] were established.

These are shown in Fig.5. In order to validate our measurements, we have indicated the species observed in our DMC pyrolysis manipulations at 300°C (in green). Fig.5a) shows that except for CH_2O, all gas species present in the DMC pyrolysis reaction scheme were identified in our experiments of DMC pyrolysis at 300°C. The DMC pyrolysis reaction scheme thus seems to be validated by the experiments carried out here. The pyrolysis of EMC at 300°C creates many species and thus has many potential thermal degradation reaction pathways. Fig.5b) shows that except for CH_2O and $CH_3OC(=O)H$, all the gaseous species present in the EMC pyrolysis reaction scheme that we proposed were identified in the experimental pyrolysis manipulations of EMC at 300°C. CH_2O and $CH_3OC(=O)H$ result from the decomposition of DMC according to the reactions *R3* and *R7*. $CH_3OC(=O)H$ is formed in small amounts in the DMC pyrolysis tests; it is also possible that it is formed in amounts that are too small to be detected in the EMC pyrolysis tests. As stated in the previous section, it is also possible that the thermal decomposition of $CH_3OC(=O)H$ preferentially occurs according to reaction *R6* to form CH_3OH and CO. The EMC pyrolysis reaction scheme proposed in Fig.5b) thus seems to be validated by the observations of the EMC pyrolysis tests carried out in our study. The stable species detected in the DMC and EMC thermal degradation manipulations and those listed in the reaction schemes established from the thermal degradation reactions in the literature are therefore consistent.

5. Comparison with global overcharge tests

In order to measure the contribution of solvent vapour thermal degradation to the emissions of the Li-ion cell, this section is devoted to the qualitative and quantitative comparison of the gases identified in the emissions from the overcharged study cell [22] and those identified in the pyrolysis of the volatile solvents DMC and EMC at 300°C in the gaseous phase over a heating time of 30min (this study). We made these comparisons with the pyrolysis manipulations performed at 300°C for 30min, since this is the condition that is the closest to the conditions observed during the overcharge tests, as reported in the studies by Yuan et al. [17] and Leising et al. [50].

5.1. Qualitative aspects

The species identified in this study and those identified in our previous study [22] are compared in Table 7. This comparison shows that: i) all the gaseous species identified in the DMC pyrolysis tests at 300°C were also present in the global tests [22]; (ii) the gaseous species observed during the thermal degradation of EMC at 300°C were also identified in the overall tests, except for DEC, diethyl ether ($C_2H_5OC_2H_5$) and methyl ethyl ether ($CH_3OC_2H_5$). The VARIAN CP-4900 µ-GC used to analyse the cell fumes during the overcharge tests does not have a column that can analyse carbonate molecules, so the possible presence of DEC could not be verified in these analyses. On the other hand, the SRA µ-GC/SM has an OV1 analysis column that allows carbonates to be analysed and that made it possible to detect and quantify the DEC in the pyrolysis tests. It is possible that the $C_2H_5OC_2H_5$ and the $CH_3OC_2H_5$ were formed during overcharge tests with typical behaviour, but in insufficient quantities to distinguish them from background noise. This was the case for $CH_3C(=O)H$, which was produced in quantities that were too small to clearly distinguish it from background noise in the overcharge tests, but that was identified *a posteriori*.

5.2. Quantitative aspects

To carry out the quantitative comparison, the emitted gas proportions extrapolated to a dummy cell containing 70% of DMC and 30% of EMC (ratio of the gaseous phase of the study cell) thermally degraded at 300°C were used. Fig.6 shows the comparison between the gaseous emissions resulting from the overcharged study cell (in blue) and those measured during the pyrolysis of a dummy cell containing 70% of DMC and 30% of EMC (in red). From Fig.6, the following observations can be made:

- All of the non-fluorinated species resulting from the thermal degradation of the DMC and EMC solvents at 300°C were identified in the overall emissions of the study cell subjected to the overcharge.
- CO_2, CH_4 and CH_3OH are species formed in almost identical proportions by the thermal degradation of DMC and EMC.

- H_2, CO and CH_3OCH_3 are species formed in greater proportions by the thermal degradation of DMC than by that of EMC.
- C_2H_4, C_2H_5OH and C_2H_6 were observed only in the EMC pyrolysis manipulations.
- The dummy cell, consisting of DMC and EMC in the ratio of the study cell gas phase, became thermally degraded at 300°C for 30min, and produced, in comparison to the overcharged study cell: i) comparable proportions (≈) of CH_4, C_2H_6, CO_2 and H_2; ii) lower proportions (<) of C_2H_4, C_3H_6 and $CH_3OC(=O)H$; iii) higher proportions (>) of CO, CH_3OCH_3, C_2H_5OH, CH_3OH and $CH_3C(=O)H$.

5.3. Discussion

The comparisons presented above make it possible to formulate the following remarks and hypotheses:

- C_2H_4 and C_2H_6 are observed in smaller quantities in the dummy cell compared to the overcharge tests. The production of these two species was observed only during the EMC pyrolysis, but they were described by Sun et al.(2016) [32] in their DMC pyrolysis mechanism. These species can therefore also be formed during DMC pyrolysis as shown in the study cell at a higher temperature than 300°C. If the internal temperature of the cell exceeds 300°C, it can be assumed that the proportions of C_2H_4 and C_2H_6 produced by the pyrolysis of EMC can be increased compared to the proportions obtained at 300°C, because it was observed that the proportion of C_2H_4 increases between 240 and 300°C, and that C_2H_6 appears as from 300°C.
- The C_2H_5OH observed during the pyrolysis of the EMC and the CH_3OH observed during the pyrolysis of the EMC and the DMC are produced in greater quantity in the dummy cell compared to the overcharge tests. It is possible that the addition of $LiPF_6$ decreases the production of C_2H_5OH in comparison with the thermal degradation of the EMC alone and allows the formation of C_2H_5F. By analogy, the production of CH_3OH observed during the thermal degradation of DMC and EMC could be decreased in the presence of fluorinated species in the electrolyte, which could allow the formation of CH_3F.
- The $CH_3OC(=O)H$ observed in the global overcharge tests is measured in a lower quantity in the pyrolysis tests of volatile solvents. This species was mentioned in the pyrolysis mechanism of Sun et al.(2016) [32]. It is possible that this species is formed at a higher temperature, or that it may have been broken down mainly in the pyrolysis tests, where the heating time is longer than that observed in the overall tests. It is also possible that this minority species is formed by the onset of the thermal degradation of the cyclic solvents.
- $CH_3C(=O)H$ is formed in a small amount during the EMC pyrolysis at all three study temperatures, but its proportion increases with the degradation temperature.
- The more the degradation temperature increases (for the same duration), the more the composition of the corresponding emission approaches that of the study cell subjected to overcharge. It has been shown by several authors [31, 51] that $LiPF_6$ catalyses the degradation

reactions; this means that the reactions observed at 300°C in our study could occur at lower temperatures in the presence of $LiPF_6$.

These observations lead us to conclude that the thermal degradation of the volatile solvents is partly responsible for the creation of the gases observed during overcharge of the study cell.

6. Conclusion

In our study, the cell was decomposed into its constituents, in order to decouple the phenomena responsible for the creation of gases, with the purpose of understanding the reaction mechanisms responsible for creating gases within the cell. An examination of the existing literature identified the main chemical reactions that can contribute to the formation of species in the gaseous phase from the constituent elements of a Li-ion cell subjected to abusive conditions. This review of the literature showed that the graphite anode and the $LiFePO_4$ cathode are thermally stable at the temperatures assumed in the overcharge tests and, therefore, do not contribute directly to the production of gaseous species. This made it possible to target the thermal degradation of the electrolyte as potentially responsible for the creation of gas. A literature review of the studies relating to the thermal degradation of solvents and/or electrolytes with gas analysis showed that these studies are few in number and that the results are inconsistent. We therefore focused on the implementation of an experimental method to study the thermal degradation of solvents in the electrolyte of the study cell. The preliminary study of the saturating vapour pressures of the cell solvents showed that the gaseous phase of the cell consists almost entirely of DMC and EMC. A DSC study in an inert and confined medium showed that the volatile solvents DMC and EMC degrade first, compared to the other two non-volatile solvents, during an increase in temperature that can be likened to a thermal runaway type event. The study of the thermal degradation of the volatile solvents DMC and EMC was thus carried out. An assembly was developed, allowing these solvents to be heated in the gaseous phase and under an inert atmosphere at several temperatures (180°C/240°C/300°C) and for several durations (30min/1h/2h) and allowing the gaseous decomposition products to be quantified by chromatography. The thermal degradations of DMC and EMC were thus carried out and the decomposition products were quantified. We found that the higher the degradation temperature, between 180 and 300°C, the more similar the composition of the gaseous phase analysed is to that of the study cell subjected to the overcharge. All of the non-fluorinated species resulting from the thermal degradation of the DMC and EMC solvents at 300°C under an inert atmosphere were identified in the overall emissions of the study cell subjected to the overcharge. The thermal degradation of DMC essentially forms CO_2, CH_3OCH_3, CO and H_2 at 300°C, at which temperature its degradation is maximal. The observed tendency is summarized in table 8. This study showed that the same gaseous species were identified in both types of tests: the global overcharge tests carried out on the cell and the thermal degradation tests carried out on the volatile solvents DMC and EMC. It can thus be concluded that the thermal degradation of the volatile solvents DMC and EMC contributes to the production of the gases observed during the overcharge of the study cell. The original results obtained in this study show that the volume and nature of the gases produced during the deconfinement of the cell are strongly related to thermal runaway.

Acknowledgements

The authors thank the “Conseil Régional du Centre Val de Loire”, France, which contributed to the financial support of this work.

References

[1] C. Hendricks, N. Williard, S. Mathew, M. Pecht, A failure modes, mechanisms, and effects analysis (FMMEA) of lithium-ion batteries , Journal of Power Sources, 297, (2015), 113-120.

[2] K. Kumai, H. Miyashiro, Y. Kobayashi, K. Takei, R. Ishikawa, Gas generation mechanism due to electrolyte decomposition in commercial lithium-ion cell, Journal of Power Sources, 81-82, (1999), 715-719.

[3] W. Kong, H. Li, X. Huang, L. Chen, Gas evolution behaviors for several cathode materials in lithium-ion batteries, Journal of Power Sources, 142, (2005), 285-291.

[4] D.H. Doughty, E.P. Roth, C.C. Crafts, G. Nagasubramanian, G. Henriksen, K. Amine, Effects of additives on thermal stability of Li ion cells, Journal of Power Sources, 146, (2005, 116-120.

[5] T. Ohsaki, T. Kishi, T. Kuboki, N. Takami, N. Shimura, Y. Sato, M. Sekino, A. Satoh, Overcharge reaction of lithium-ion batteries, Journal of Power Sources, 146, (2005), 97-100.

[6] D.P. Abraham, E.P. Roth, R. Kostecki, S. MacLaren, D.H. hty, Diagnostic examination of thermally abused high-power lithium-ion cells, Journal of Power Sources, 161, (2006), 648 – 657.

[7]: H.-F. Li, J.-K. Gao, S.-L. Zhang, Effect of overdischarge on swelling and recharge performance of lithium ion cells, Chinese Journal of Chemistry, 26, (2008), 1585-1588.

[8] E.P. Roth, Abuse response of 18650 Li-ion Cells with different cathodes using EC:EMC/$LiPF_6$ and EC:PC:DMC/$LiPF_6$ electrolytes, ECS Transactions, 11, 19, (2008), 19-41.

[9] P. Ribière, S. Grugeon, M. Morcrette, S. Boyanov, S. Laruelle, G. Marlair, Investigation on the fire-induced hazards of Li-ion battery cells by fire calorimetry Energy Environmental Science, 5, (2011), 5271-5280.

[10] G. Gachot, S. Grugeon, I. Jimenez-Gordon, G.G. Eshetu, S. Boyanov, A. Lecocq, G. Marlair, S. Pilard, S. Laruelle, Gas chromatography/Fourier transform infrared/ mass spectrometry coupling: a tool for Li-ion battery safety field investigation, Analytical Methods, 6, (2014), 6120-6124.

[11] A.W. Golubkov, D. Fuchs, J. Wagner, H. Wiltsche, C. Stangl, G. Fauler, G. Voitic, A. Thaler, V. Hacker, Thermal-runaway experiments on consumer Li-ion batteries with metal-oxide and olivin-type cathodes, RSC Advances, 4, (2014), 3633-3642.

[12] F. Larsson, P. Andersson, P. Blomqvist, A. Lorén, B.-E. Mellander, Characteristics of lithium-ion batteries during fire test, Journal of Power Sources, 271 (2014), 414-420.

[13] V. Somandepalli, K.C. Marr, Q. Horn, Quantification of Combustion Hazards of Thermal Runaway Failures in Lithium-Ion Batteries, SAE International Journal of Alternative Powertrains, 3, 1, (2014), 98-104.

[14] Y. Fu, S. Lu, K. Li, C. Liu, X. Cheng, H. Zhang, An experimental study on burning behaviors of 18650 lithium ion batteries using a cone calorimeter, Journal of Power Sources, 273, (2015), 216-222.

[15] N.S. Spinner, C.R. Field, M.H. Hammond, B.A. Williams, K.M. Myers, A.L. Lubrano, S.L. Rose-Pehrsson, S.G. Tuttle, Physical and chemical analysis of lithium-ion battery cell-to-cell failure events inside custom fire chamber, Journal of Power Sources, 279, (2015), 713-721.

[16] A.W. Golubkov, S. Scheikl, R. Planteu, G. Voitic, H. Wiltsche, C. Stangl, G. Fauler, A.Thalera, V. Hacker, Thermal runaway of commercial 18650 Li-ion batteries with LFP and NCA cathodes – impact of state of charge and overcharge, RSC Advances, 5, (2015), 57171.

[17]: Q. F. Yuan, F. Zhao, W. Wang, Y.Zhao, Z. Liang, D. Yan, Overcharge failure investigation of lithium-ion batteries, Electrochimica Acta, 178 (2015), 682–688.

[18] J. Sun, J. Li, T. Zhou, K. Yang, S. Wei, N. Tang, N. Dang, H. Li, X. Qiu, L. Chen, Toxicity, a serious concern of thermal runaway from commercial Li-ion battery, Nano Energy, 27, (2016), 313-319.

[19] Y. Zheng, K. Qian, D. Luo, Y. Li, Q. Lu, B. Li, Y.-B. He, X. Wang, J. Li, F. Kang, Influence of over-discharge on the lifetime and performance of $LiFePO_4$/graphite batteries, RSC Advances, 6, (2016), 30474–30483.

[20] M. Lammer, A. Königseder, V. Hacker, Holistic methodology for characterisation of the thermally induced failure of commercially available 18650 lithium ion cells, RSC Advances, 7, (2017), 24425-24429.

[21] F. Larsson, P. Andersson, P. Blomqvist, B.-E. Mellander, Toxic fluoride gas emissions from lithium-ion battery fires, Nature, 7: 10018, (2017).

[22] Y. Fernandes, A. Bry and S. de Persis, Identification and quantification of gases emitted during abuse tests by overcharge of a commercial Li-ion battery, Journal of Power Sources, Volume 389, 15 June 2018, Pages 106-119

[23] C. Delacourt, P. Poizot, J-M. Tarascon, C. Masquelier, The existence of a temperature-driven solid solution in Li_xFePO_4 for $0 \leq x \leq 1$, Nature Materials, 4, (2005), 254-260.

[24] S. P. Ong, A. Jain, G. Hautier, B. Kang, G. Ceder, Thermal stabilities of delithiated olivine MPO_4 (M = Fe, Mn) cathodes investigated using first principles calculations, Electrochemistry Communications, 12, (2010), 427–430.

[25] M.H.J. Wijnen, Decomposition of dimethyl carbonate on quartz, The Journal of Chemical Physics, 34, (1961), 1465.

[26] J.C.J. Thynne, P. Gray, The Methyl-Radical-Sensitized Decomposition of Gaseous Dimethyl Carbonate, Transactions of the Faraday Society, 58, (1962), 2403.

[27] A.S. Gordon, W.P. Norris, A Study of the Pyrolysis of Methyl Ethyl and Diethyl Carbonates in the Gas Phase, The Journal of Physical Chemistry, 69, (1965), 3013-3017.

[28] G-G. Botte, T-J. Bauer, MRSST a new method to evaluate thermal stability of electrolytes for lithium ion batteries, Journal of Power Sources, 119-121, (2003), 815–820.

[29] B.Ravdel, K.M. Abraham, R. Gitzendanner, J. DiCarlo, B.Lucht, C. Campion, Thermal stability of lithium-ion battery electrolytes, Journal of Power Sources, 119–121, (2003), 805–810.

[30] J.S. Gnanaraj, E. Zinigrad, L. Asraf, H.E. Gottlieb, M. Sprecher, M. Schmidt, W. Geissler, D. Aurbach, A detailed investigation of the thermal reactions of $LiPF_6$ solution in organic carbonates using ARC and DSC, Journal of the Electrochemical Society, 150, 11, (2003), A1533-A1537.

[31] J. Lamb, C.J. Orendorff, E.P.Roth, J. Langendorf, Studies on the Thermal Breakdown of Common Li-Ion Battery Electrolyte Components, Journal of the Electrochemical Society, 162, 10, (2015), A2131-A2135.

[32] W. Sun, B. Yang, N. Hansen, C.K. Westbrook, F. Zhang, G. Wang, K. Moshammer, C.K. Law, An experimental and kinetic modeling study on dimethyl carbonate (DMC) pyrolysis and combustion, Combustion and Flame, 164, (2016), 224–238.

[33] W. Sun, C. Huang, T. Tao, F. Zhang, N. Hansen, B. Yang, Exploring the high temperature kinetics of diethyl carbonate (DEC) under pyrolisis and flame conditions, Combustion and Flame, 181, (2017), 71-81.

[34] S. Bertilsson, F. Larsson, M.Furlani, I. Albinsson, B-E. Mellander, Lithium-ion battery electrolyte emissions analyzed by coupled thermogravimetric/Fourier-transform infrared spectroscopy, Journal of Power Sources, 365, (2017), 446-455.

[35] X. Zhang, J. Zuo, C. Jian, Experimental Isobaric Vapor-Liquid Equilibrium for Binary Systems of Ethyl Methyl Carbonate + Methanol, + Ethanol, + Dimethyl Carbonate, or + Diethyl Carbonate at 101.3 kPa, Journal of Chemical & Engineering data, 55, (2010), 4896–4902.

[36] D. Kulikov, S. P. Verevkin, A. Heintz, Enthalpies of vaporization of a series of aliphatic alcohols. Experimental results and values predicted by the ERAS-model, Fluid Phase Equilibria, 192, (2001), 187–207.

[37] J.C. Brocard, F. Baronnet, Effets de parois dans la pyrolyse du méthyl tert-butyl éther (MTBE), Journal de chimie physique, 84, 1, (1987), 19-25.

[38] J.F. Foucaut, R. Martin, Wall Effects in the Pyrolysis of Diethylether. A Case of HeteroHomogeneous Pyrolysis at 500°C, International Journal of Chemical Kinetics, 11, 7, (1979), 789-798.

[39] S. Hess, M. Wohlfahrt-Mehrens, M. Wachtler, Flammability of Li-Ion Battery Electrolytes: Flash Point and Self-Extinguishing Time Measurements, Journal of the Electrochemical Society, 162, 2, (2015), A3084-A3097.

[40] C.N. Hinshelwood, P.J. Askey, Homogeneous reactions involving complex molecules. The kinetics of the decomposition of gaseous dimethyl ether, Proceedings of the royal society, 115, 770, (1927).

[41] H. Li, M. Wen, Z-X. Wang, Computational mechanistic study of the hydrogenation of carbonate to methanol catalyzed by the Ru^{II}PNN complex, Inorganic Chemistry, 51, (2012), 5716−5727.

[42] T. Choi, H. Stenger, Kinetics of methanol decomposition and water gas shift reaction on a commercial Cu-ZnO/Al_2O_3 catalyst, Fuel Chemistry Division Preprints, 47, 2, (2002), 723.

[43] J.S. Francisco, Mechanistic Study of the Gas-Phase Decomposition of Methyl Formate, American Chemical Society, 125, (2003), 10475-10480.

[44] E.W.R. Steacie, The Kinetics of the Heterogeneous Thermal Decomposition of Methyl Formate, Proceedings of the Royal Society of London, 127, (1930), 314-330.

[45] K.J. Laidler, D.J. McKenney Kinetics and Mechanisms of the Pyrolysis of Diethyl Ether. I. The Uninhibited Reaction Proceedings of the Royal Society of London. Series A, Mathematical and Physical Sciences, 278, 1375, (1964).

[46] A. Parandaman , B. Rajakumar, Shock tube study and RRKM calculations on thermal decomposition of 2-chloroethyl methyl ether, Combustion and Flame, 186, (2017), 263-276.

[47] Y. Yoshida, Y. Arai, S. Kado, K. Kunimori, K. Tomishige, Direct synthesis of organic carbonates from the reaction of CO_2 with methanol and ethanol over CeO_2 catalysts, Catalysis Today, 115, (2006), 95-101.

[48] Y. Sekine, M. Tomioka, M. Matsukata, E. Kikuchi, Catalytic degradation of ethanol in an electric fiel, Catalysis Today, 146, (2009), 183–187.

[49] J.M. Church, H.K. Joshi, Acetaldehyde by dehydrogenation of ethyl alcohol, Industrial and Engineering Chemistry, 43, 8, (1951), 1804-1811.

[50] R.A. Leising, M.J. Palazzo, E.S. Takeuchi, K.J. Takeuchi, A study of the overcharge reaction of lithium-ioin batteries, Journal of Power Sources, 97-98, (2001), 681-683.

[51] C.K. Park, R. Rubino, Thermally Stable Electrolyte for Lithium Ion Batteries, ECS Transactions, 58, 26, (2014), 1-9.

Figure 1

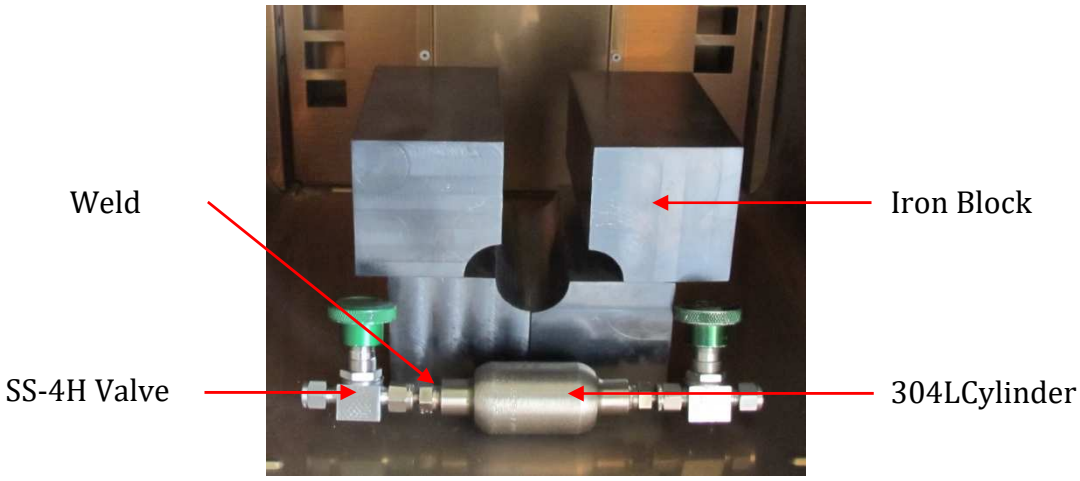

Figure 2

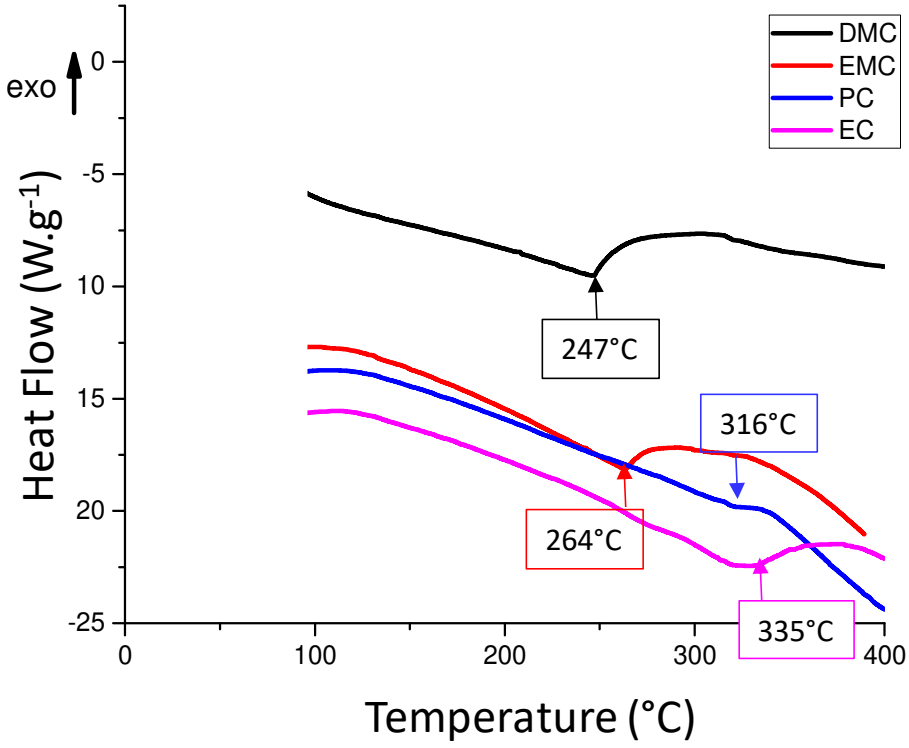
DMC
EMC
PC
EC
exo
Heat Flow (W.g-1)
0
-5
10
15
20
-25
0
100
200
300
400
Temperature (°C)
247°C
316°C
264°C
335°C

Figure 3

a) 180°C

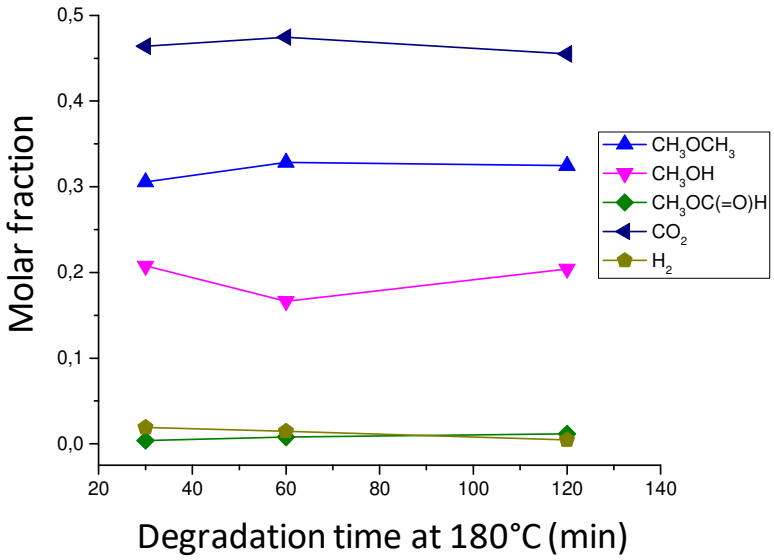

b) 240°C

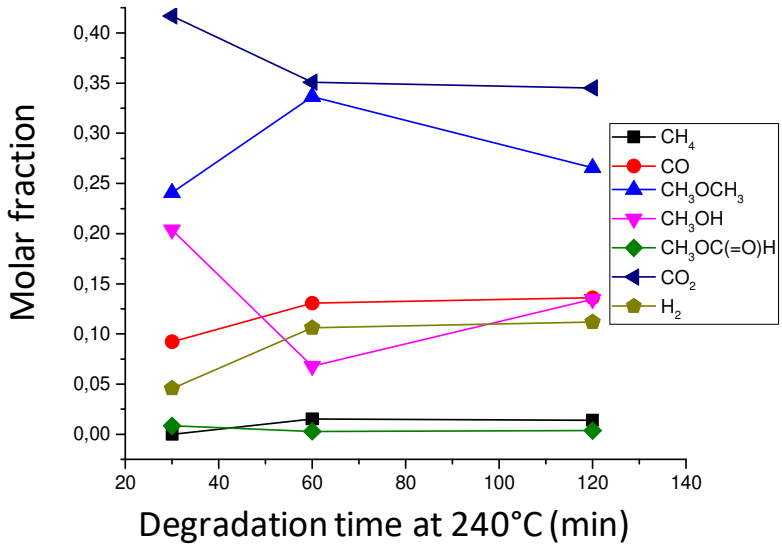
Molar fraction
0,40
0,35
0,30
0,25
0,20
0,15
0,10
0,05
0,00
20
40
60
80
100
120
140
Degradation time at 240°C (min)
CH4
CO
CH3OCH3
CH3OH
CH3OC(=O)H
CO2
H2

c) 300°C

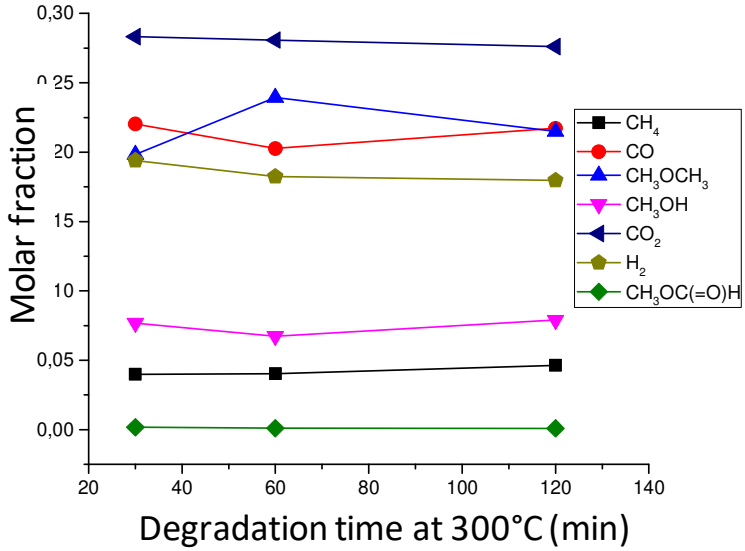
Molar fraction
0,30
0,25
20
15
10
0,05
0,00
20
40
60
80
100
120
140
Degradation time at 300°C (min)
CH4
CO
CH3OCH3
CH3OH
CO2
H2
CH3OC(=O)H

Figure 4

a) 180°

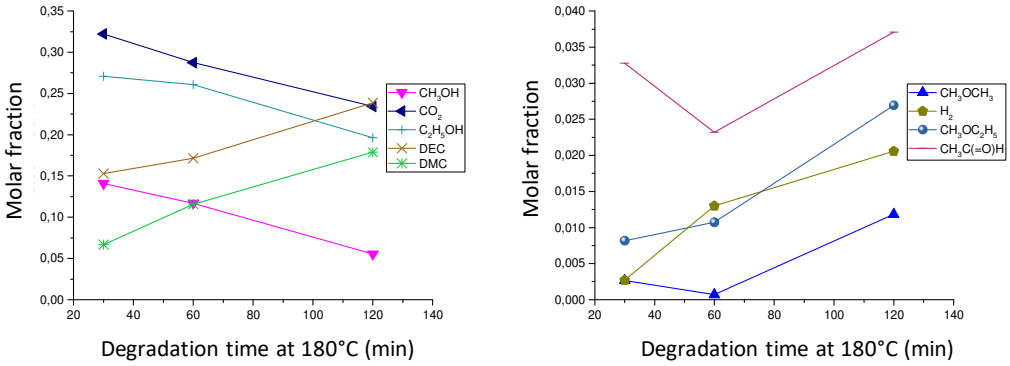

b) 240°C

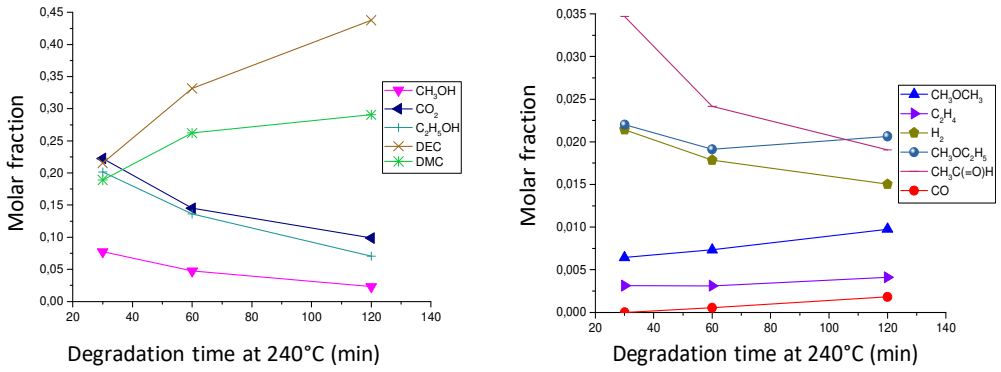

c) 300°C

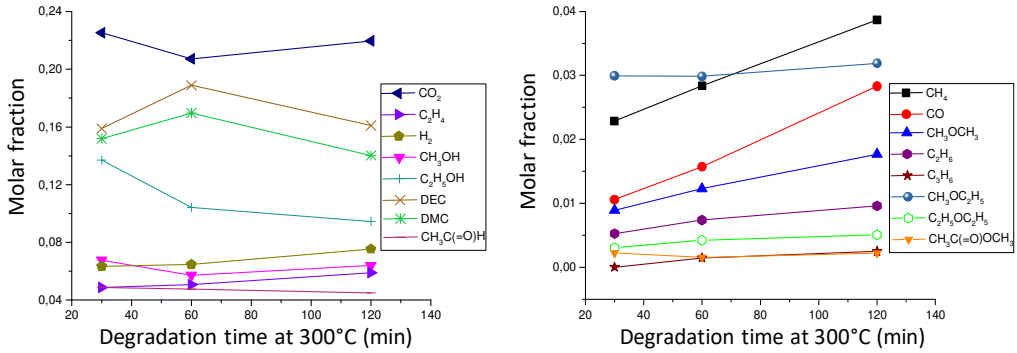

Figure 5

a)

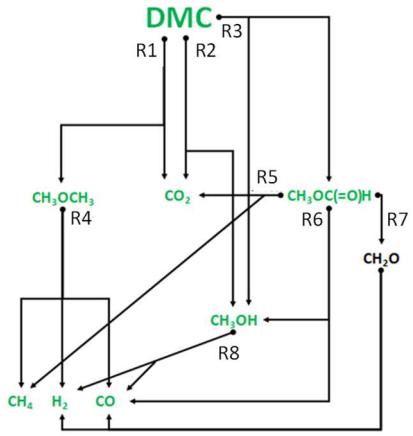

b)

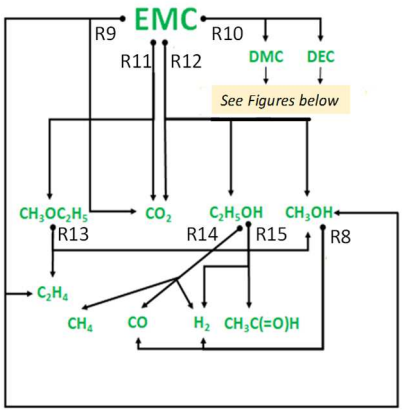

Caption with reference

R1: [25]
R2: [25]
R3: [41]
R4: [40]
R5: [43]
R6: [44]
R7: [44]
R8: [42]
R9: [27]
R10: [29]
R11: [30]
R12: [47]
R13: [46]
R14: [48]
R15: [49]
R16: [30]
R17: [45]
R18: [45]

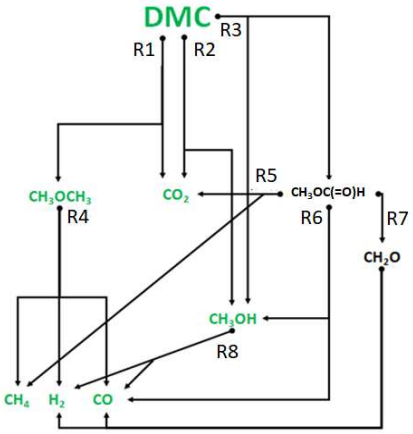

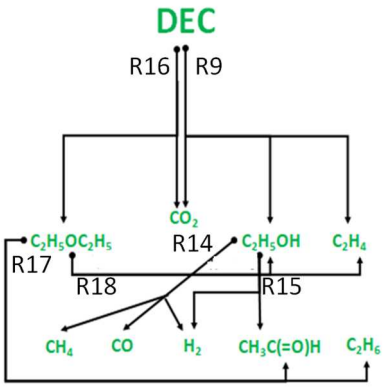

Figure 6

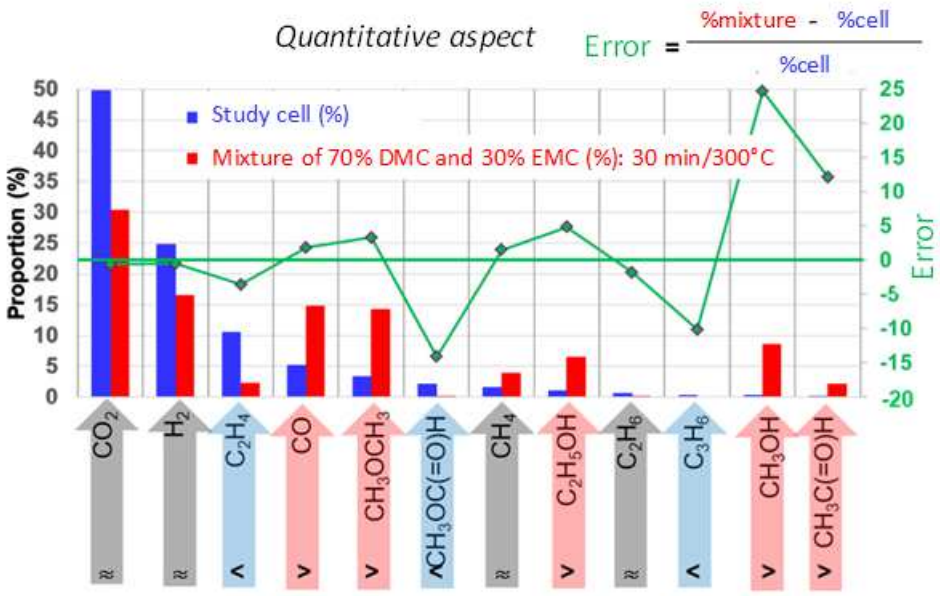
Quantitative aspect
Error = %mixture - %cell / %cell
Study cell (%)
Mixture of 70% DMC and 30% EMC (%): 30 min/300°C
Proportion (%)
Error
50
45
40
35
30
25
20
15
10
5
0
25
20
15
10
5
0
-5
-10
-15
-20
CO_2
H_2
C_2H_4
CO
CH_3OCH_3
$CH_3OC(=O)H$
CH_4
C_2H_5OH
C_2H_6
C_3H_6
CH_3OH
$CH_3C(=O)H$
≈
≈
<
>
>
>
≈
>
≈
<
>
>

Table 1

	MS5A column under helium	OV1 column under helium	PLOTQ column under helium	MS5A column under argon
Column temperature (°C)	80	46	85	80
Pressure of the column (bar)	1.93	1.10	1.10	2.07

Table 2

Condition	n(O)/n(C) ratio in the sum of the products created	n(H)/n(C) ratio in the sum of the products created
30min/180 °C	1.12	2.11
1h/180 °C	1.11	2.04
2h/180 °C	1.10	2.12
30min/240 °C	1.15	1.97
1h/240 °C	1.00	2.07
2h/240 °C	1.06	2.08
30min/300 °C	1.04	2.00
1h/300 °C	1.00	2.07
2h/300 °C	1.01	2.04
Mean ± standard deviation	1.07 ± 0.05	2.05 ± 0.05

Table 3

Condition	DMC loss (%)
30min/180 °C	1.12
1h/180 °C	1.56
2h/180 °C	3.12
30min/240 °C	3.46
1h/240 °C	6.09
2h/240 °C	10.58
30min/300 °C	13.24
1h/300°C	24.19
2h/300°C	42.13

Table 4

Condition	n(O)/n(C) in the sum of the products created	n(H)/n(C) in the sum of the products created
30min/180°C	0.85	2.10
1h/180°C	0.84	2.10
2h/180°C	0.79	2.05
30min/240°C	0.80	2.09
1h/240°C	0.76	2.05
2h/240°C	0.73	2.02
30min/300°C	0.78	2.06
1h/300°C	0.76	2.05
2h/300°C	0.76	2.06
Mean ± standard deviation	0.79 ± 0.04	2.06 ± 0.02

Table 5

Conditions	EMC loss (%)
30min/180°C	2.50
1h/180°C	3.92
2h/180°C	5.43
240°C/30min	11.43
240°C/1h	25.30
240°C/2h	49.17
30min/300°C	26.94
1h/300°C	48.42
2h/300°C	70.11

Table 6

Pyrolysis temperature >	180°C		240°C		300°C	
Precursor >	DMC	EMC	DMC	EMC	DMC	EMC
$CH_3OC(=O)H$						
H_2						
CH_3OCH_3						
CO_2						
CO						
CH_3OH						
CH_4						
$CH_3C(=O)OCH_3$						
C_2H_4						
$CH_3C(=O)H$						
$C_2H_5OC_2H_5$						
$CH_3OC_2H_5$						
C_2H_5OH						
C_2H_6						
C_3H_6						
DMC						
DEC						

Table 7

Identified species

Unidentified species

Gaseous species	DMC emission 30 min/300°C	EMC emission 30 min/300°C	DMC + EMC 30min/300°C	Emissions from the study cell
CO_2				
H_2				
C_2H_4				
CO				
CH_3OCH_3				
$CH_3OC(=O)H$				
CH_4				
C_2H_5OH				
C_2H_6				
C_3H_6				
CH_3OH				

Table 8:

Decomposition product	DMC 180°C - 300°C	EMC 180°C - 300°C
H_2	+	+
CO	+	+
CO_2	-	-
CH_4	+	+
CH_3OH	-	-
CH_3OCH_3	-	=
$CH_3C(=O)H$		=
C_2H_5OH		-
DMC		=
DEC		=
C_2H_4		+